ADVANCED MATERIALS INTERFACES
Open Access

Supporting Information

for *Adv. Mater. Interfaces*, DOI 10.1002/admi.202300249

Atomistic Understanding of the Coherent Interface Between Lead Iodide Perovskite and Lead Iodide

Mathias Uller Rothmann, Kilian B. Lohmann, Juliane Borchert, Michael B. Johnston, Keith P. McKenna, Laura M. Herz and Peter D. Nellist**

Atomistic Understanding of the Coherent Interface Between Lead Iodide Perovskite And Lead Iodide - Supporting Information

Mathias Uller Rothmann,[†,‡] Kilian B. Lohmann,[†] Juliane Borchert,[†] Michael B. Johnston,[†] Keith McKenna,[¶] Laura M. Herz,[*,†,§] and Peter D. Nellist[*,‡]

†*Department of Physics, University of Oxford, Clarendon Laboratory, Parks Road, Oxford OX1 3PU, UK*

‡*Department of Materials, University of Oxford, Parks Road, Oxford OX1 3PH, UK*

¶*Department of Physics, University of York, Heslington, York YO10 5DD, UK*

§*Institute for Advanced Study, Technical University of Munich, Lichtenbergstrasse 2a, D-85748 Garching, Germany*

E-mail: laura.herz@physics.ox.ac.uk; peter.nellist@materials.ox.ac.uk

Methods

Sample preparation

$FAPbI_3$ thin films were deposited on the carbon-coated side of 300-mesh copper TEM grids. Immediately prior to deposition, the grids were O_2-plasma cleaned for 0.3 minutes.

$CH(NH)_2I$ (FAI) and PbI_2 were co-evaporated in a customised thermal evaporation chamber described previously.[1] Heating of the sources started once the chamber pressure fell below 5×10^{-6} mbar. The PbI_2 rate was kept constant at 0.23 Å/s, measured using a gold-plated quartz microbalance (QMB). This FAI crucible temperature was kept around 150 °C during deposition. During deposition, the pressure increased to 1-2$\times10^{-5}$ mbar. The duration of the overall perovskite deposition was controlled such that the film thickness was 90 nm. After deposition, the films were annealed at 170 °C for 1 min. The films were stored in a nitrogen-filled glove box after preparation and transported to the microscope in a triple-sealed nitrogen atmosphere to prevent exposure to moisture. All samples were loaded rapidly into the microscope, being in contact with air for less than a minute.

Perovskite film thicknesses were determined from calibration of material deposition rates of the two sources according to quartz microbalance readings inside the vacuum chamber, supported by film depositions on hard transparent quartz substrates for which film thickness readings were determined from a combination of Dektak profilometer readings and optical transmission measurements.

Image acquisition

Microscopy was performed on a JEOL ARM-200F cold FEG, Cs probe corrected STEM at 200 kV acceleration voltage, 23-24 mrad convergence angle, using an annular dark field detector at 8 cm camera length, resulting in inner and outer collection angles of 33 and 120.77 mrad, respectively for LAADF imaging. Both room temperature and cryogenic conditions were used, and the cryogenic conditions did not noticeably reduce the beam sensitivity of the $FAPbI_3$

thin films, so all imaging was done at room temperature. Similarly, no noticeable difference in beam sensitivity was found between 200 and 300 kV acceleration voltage. All imaging presented in the manuscript was at 200 kV. All alignments and focusing were done away from the areas imaged to reduce electron beam-induced damage to the material. All micrographs were obtained without tilting the sample to reduce the beam damage.

Diffraction simulation

Simulations of the SAED and XRD patterns were performed using commercial CrystalDiffract and SingleCrystal software and were based on 2H PbI_2 (ICSD number 68819), cubic $FAPbI_3$ (found at `https://github.com/WMD-group/hybrid-perovskites/blob/fe4b188d5c7549050d9994c64b` `2014_cubic_halides_PBEsol/FAPbI3.cif`), and 3R PbI_2 (available for download with this paper).

Theoretical calculations

First principles density functional theory calculations were performed using the projector augmented wave method which is implemented in the Vienna Ab initio Simulation Package (VASP).[2,3] Calculations for the bulk $FAPbI_3$ and PbI_2 phases are carried with two different approximations for the exchange-correlation functional: the generalized gradient approximation functional PBESol and the hybrid functional HSE06[4] (with 40% Hartree-Fock exchange and spin-orbit coupling included along with the D3 Grimme dispersion correction to describe the Van der Waals interactions[5], hereafter HSE+D3+SOC). We consider β-$FAPbI_3$ rather than the room temperature cubic $FAPbI_3$ phase for constructing the interfaces models. β-$FAPbI_3$ is predicted to be stable below room temperature and is slightly tetragonally distorted structure.[6] This has the advantage that the FA molecules orient in preferred directions preventing issues associated with rotational disorder one often finds in simulations of interface defects with the cubic phase. The bulk β-$FAPbI_3$ unit cell was optimized at the PBESol level using a $6 \times 6 \times 4$ gamma centered k-point grid for Brillouin zone sampling and a 500 eV plane wave cut-off until all forces are less than 0.01 eVÅ^{-1} yielding lattice constants $a = 9.00$ and $c = 12.51$ Å and

a band gap $E_g = 1.27$ eV. This corresponds to a pseudocubic structure with $a = 6.36$ and $c = 6.23$ Å, very close to the experimental lattice constant for the room temperature phase ($c = 6.36$ Å). The trigonal PbI_2 until cell was optimized using the same plane wave cut-off and a $6 \times 6 \times 6$ k-point grid yielding $a = 7.60$ Å, $\alpha = 34.80°$ and $E_g = 2.20$ eV. A coherent interface between β-$FAPbI_3$ and PbI_2 can be produced by applying less than 1% strain (which we apply to PbI_2 as the secondary phase). The interface joins the β-$FAPbI_3$(001) surface to the PbI_2(104) surface with β-$FAPbI_3$[110] parallel to PbI_2[010]. A supercell containing ~ 25 Å thick grains of β-$FAPbI_3$ and PbI_2 with two equivalent periodically repeated interfaces and optimized using a $4 \times 4 \times 1$ k-point grid (including optimization of the cell vector perpendicular to the interfaces). The electronic density of states (DOS) projected on various regions within the supercell is then calculated to investigate whether any states are present within the β-$FAPbI_3$ band gap. The projected DOS indicates the PbI_2 and interface bands lie above and below the conduction and valence bands of β-$FAPbI_3$, respectively and the absence of any gap states. This analysis also suggests the conduction band offset between the two materials is larger than the valence band offset. Structures were visualized using the VESTA package[7].

To provide a more precise determination of the band offsets we also compute the plane averaged electrostatic potential for the supercell and align this to corresponding calculations for the separate β-$FAPbI_3$ and PbI_2 bulk phases at both the PBESol and HSE+D3+SOC levels of theory[8,9]. Using HSE+D3+SOC with structures optimized at the PBESol level of theory yields bulk band gaps of 1.07 eV (β-$FAPbI_3$) and 2.89 eV (PbI_2). The calculated valence band offsets are 0.23 eV (PBESol) and 0.50 eV (HSE+D3+SOC) and the conduction band offsets are 0.70 eV (PBESol) and 1.27 eV (HSE+D3+SOC).

References

(1) Borchert, J.; Milot, R. L.; Patel, J. B.; Davies, C. L.; Wright, A. D.; Martinez Maestro, L.; Snaith, H. J.; Herz, L. M.; Johnston, M. B. Large-area, highly uniform evaporated formamidinium lead triiodide thin films for solar cells. *ACS Energy Letters* **2017**, *2*, 2799–2804.

(2) Kresse, G.; Furthmüller, J. Efficiency of ab-initio total energy calculations for metals and

semiconductors using a plane-wave basis set. *Computational Materials Science* **1996**, *6*, 15–50.

(3) Kresse, G.; Furthmüller, J. Efficient iterative schemes for ab initio total-energy calculations using a plane-wave basis set. *Physical Review B* **1996**, *54*, 11169–11186.

(4) Krukau, A. V.; Scuseria, G. E.; Perdew, J. P.; Savin, A. Hybrid functionals with local range separation. *The Journal of Chemical Physics* **2008**, *129*, 124103.

(5) Grimme, S. Accurate description of van der Waals complexes by density functional theory including empirical corrections. *Journal of Computational Chemistry* **2004**, *25*, 1463–1473.

(6) Weber, O. J.; Ghosh, D.; Gaines, S.; Henry, P. F.; Walker, A. B.; Islam, M. S.; Weller, M. T. Phase Behavior and Polymorphism of Formamidinium Lead Iodide. *Chemistry of Materials* **2018**, *30*, 11.

(7) Momma, K.; Izumi, F. VESTA3 for three-dimensional visualization of crystal, volumetric and morphology data. *Journal of Applied Crystallography* **2011**, *44*, 1272–1276.

(8) Li, Y.-H.; Walsh, A.; Chen, S.; Yin, W.-J.; Yang, J.-H.; Li, J.; Da Silva, J. L. F.; Gong, X. G.; Wei, S.-H. Revised ab initio natural band offsets of all group IV, II-VI, and III-V semiconductors. *Applied Physics Letters* **2009**, *94*, 212109.

(9) Padilha, A. C. M.; McKenna, K. P. Structure and properties of a model conductive filament/host oxide interface in HfO_2-based ReRAM. *Physical Review Materials* **2018**, *2*, 045001.

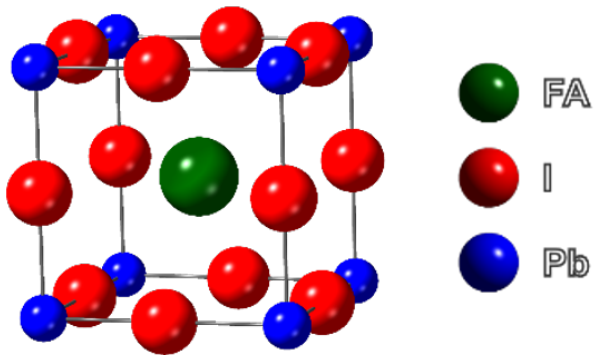

Figure S1: Schematic of the structure of cubic $FAPbI_3$.

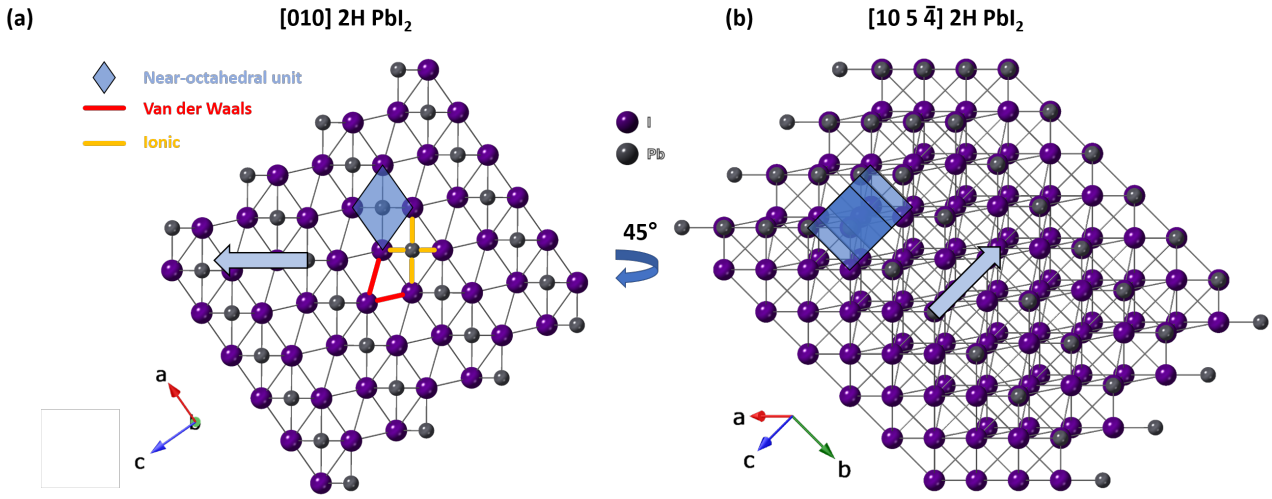

Figure S2: (a) [010]-oriented 2H PbI_2 crystal model illustrating the sheets of ionically bonded (orange bonds) near-octahedral units (light blue). The sheets themselves are bonded through Van der Waals bonding. In the 2H polytype, the I-Pb-I bonds within the near-octahedral units do not align with the I-I bonds between the sheets. (b) The same crystal model as (a) rotated 45° around the long axis of the near-octahedral rhombus. The stacking of the near-octahedral units is illustrated by slightly shifted light blue squares. The light blue arrows in (a,b) illustrate the directions, but not the magnitude, of the shifts necessary to form a polytype that interfaces coherently with cubic $FAPbI_3$.

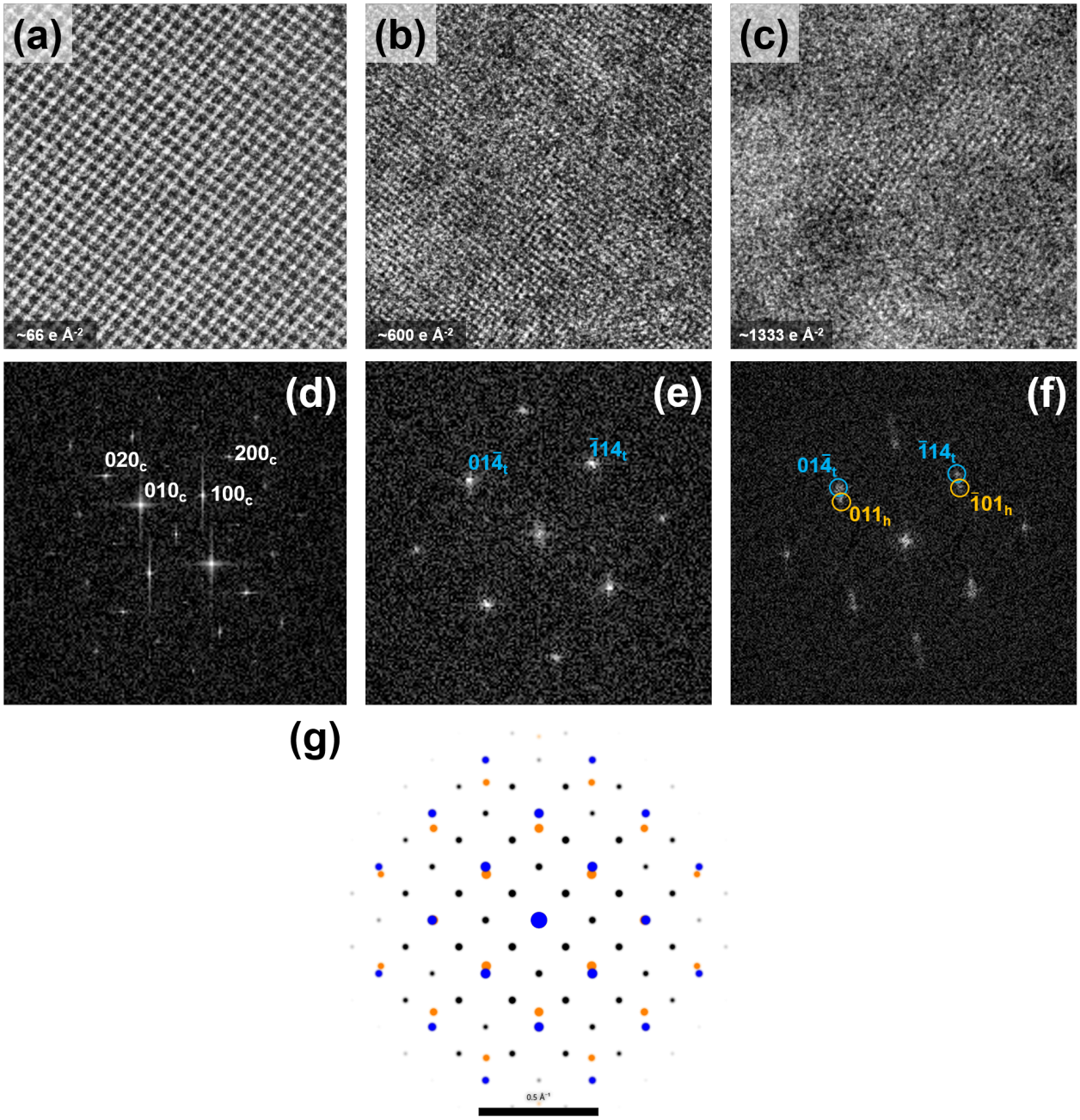

Figure S3: Different phases of a $FAPbI_3$ thin film as a function of electron dose. (a-c) show the real-space progression of a $FAPbI_3$ thin film under low-dose electron irradiation. (a) At low dose, the characteristic perovskite structure is clear. (b) After brief exposure, the contrast is a square lattice with the same orientation but half the spacing of that in (a) is observed while still maintaining a square projection. (c) Further damage reduces the lattice contrast and shows regions with a distorted lattice. (d-f) Show the corresponding Fourier transforms. (d) Initially, a pristine perovskite structure is evident. (e)The $\{100\}_c$ spots disappear after initial exposure while still maintaining a square pattern which can be indexed as the observed trigonal 3R PbI_2 denoted by the 't' subscript and matching the spacing and orientation of the $\{200\}_c$ spots. (f) After extended exposure, both trigonal 3R and hexagonal 2H (denoted by the 'h' subscript) PbI_2 is observed in the FT. (g) Simulated SAED pattern showing a superposition of [100]-oriented cubic $FAPbI_3$ (black), [841]-oriented trigonal 3R PbI_2 (blue), and $[\bar{1}0\bar{1}]$-oriented hexagonal 2H PbI_2. The geometry of the blue and orange spots corresponds very well to that in (f) and the geometry of the black and blue spots corresponds very well to that in Figure 1(b). Image adapted from Figure 2 of Reference [12]. Reprinted with permission from AAAS.

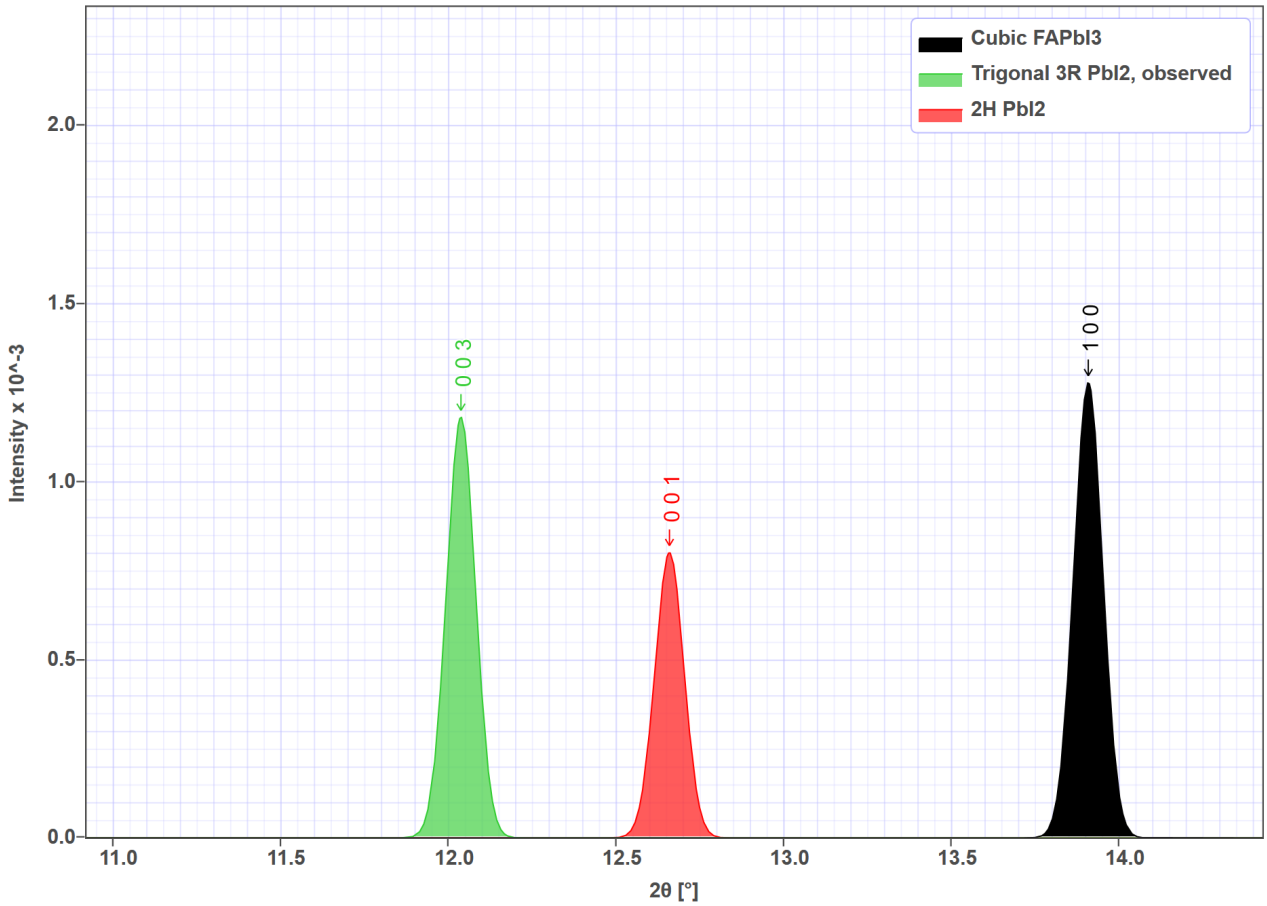

Figure S4: Closeup of the range of 11°-14° of the XRD pattern seen in Figure 4.

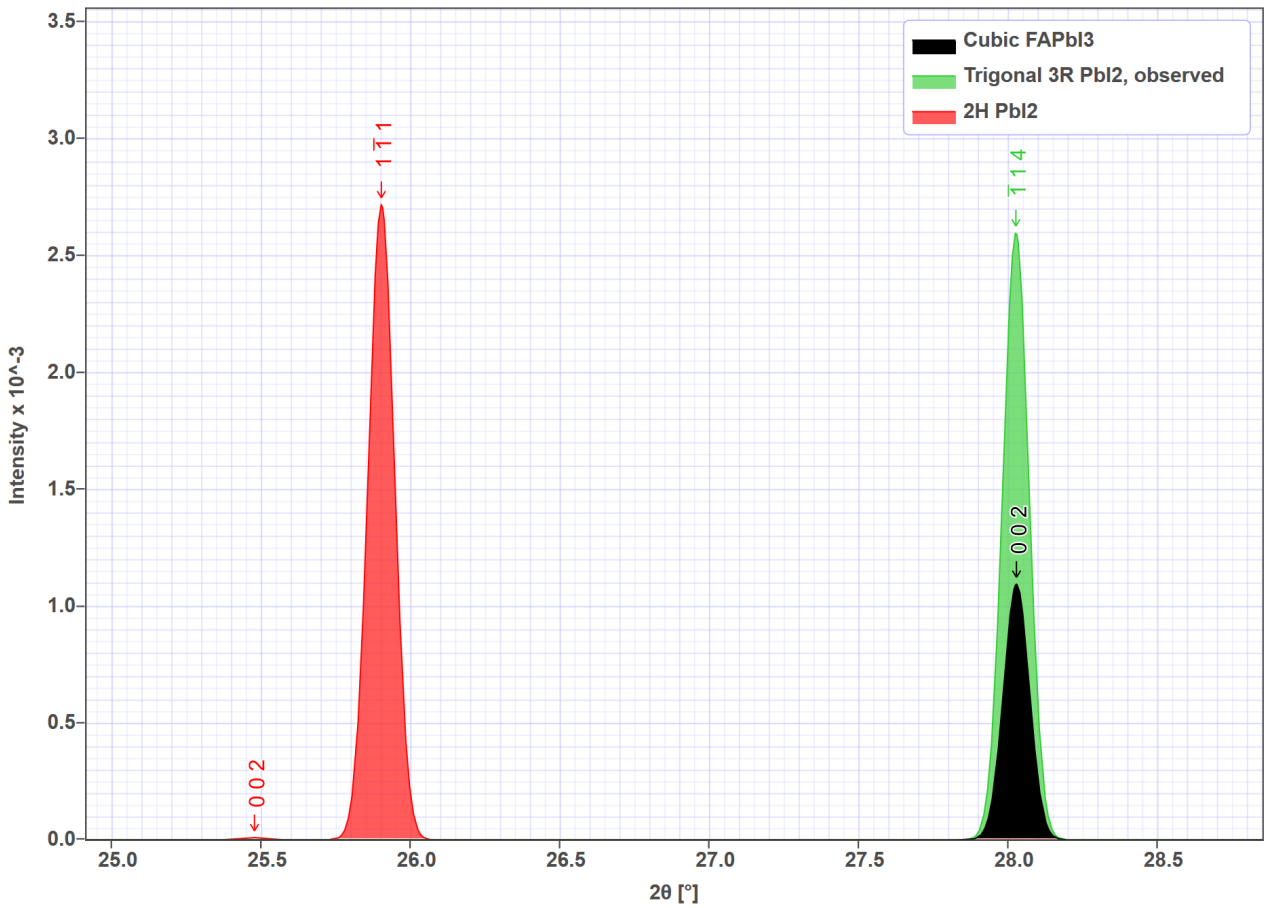

Figure S5: Closeup of the range of 25°-29° of the XRD pattern seen in Figure 4.